This article has been accepted for publication in a future issue of this journal, but has not been fully edited. Content may change prior to final publication. Citation information: DOI 10.1109/TMM.2017.2774004, IEEE Transactions on Multimedia

Efficient and Robust Image Coding and Transmission based on Scrambled Block Compressive Sensing

Zan Chen, Xingsong Hou, *Member, IEEE,* Xueming Qian, *Member, IEEE,* and Chen Gong, *Member, IEEE*

***Abstract*—Image transmission in a wireless visual sensor network (WVSN) with limited resources over an unreliable and bandwidth-limited wireless channel is challenging. This paper presents a highly efficient and robust image coding and transmission scheme with a simple encoder based on compressive sensing (CS) for WVSNs. First, an image measurement based on scrambled block compressive sampling (SBCS) with a separable sensing operator is proposed to simplify the encoder. Second, a progressive non-uniform quantization (PNQ), which exploits the measurement distribution at the encoder side and the measurement dependencies at the decoder side, is designed to improve the rate-distortion (R-D) performance while maintaining low complexity at the encoder. Third, to further improve the R-D performance, a progressive non-local low-rank (NLR) reconstruction is designed at the decoder. The experimental results show that the proposed scheme can achieve higher R-D performance compared with the benchmark CS-based image coding and transmission schemes. Higher robustness can be achieved compared with the traditional source-channel coding, such as Consultative Committee for Space Data Systems−Image Data Compression (CCSDS-IDC) with Raptor codes under a time-varying packet loss channel, and the encoding time can be significantly reduced compared with the traditional image coding schemes. The experimental results also show that the proposed scheme achieves state-of-the-art coding efficiency with lower computational complexity at the encoder while still supporting error resilience.**

I. Introduction

Wireless visual sensor networks (WVSNs) consist of low-cost and low-power visual sensor nodes, which can collect and transmit visual information for many potential applications, such as surveillance of wild animals, vehicle traffic monitoring, and healthcare monitoring [1]–[3]. Due to limited energy and bandwidth resources, the image data need to be compressed. Although embedded visual sensors are becoming powerful, some challenging problems still exist for WVSNs [4].

Image coding and transmission schemes need to find a balance between computational complexity and compression performance. Inexpensive wireless visual sensors are typically equipped with batteries of limited capacity, and therefore, they cannot sustain the heavy computations involved in visual compression and communication. HEVC and JPEG2000 are not appropriate for visual sensor nodes because these approaches achieve excellent compression performance at the cost of high computational complexity. Moreover, the CCSDS-IDC standard has sought a balance between complexity and performance, but it still incurs high computational complexity [5].

Meanwhile, image coding and transmission schemes should be robust to packet loss. Considering the limited packet size, compressed frames could be split into multiple data packets. However, if some important data packets are dropped, then the decoder is unable to reconstruct the original image. Traditionally, channel coding protection is deployed to address packet loss. Nevertheless, the additional channel coding redundancies increase the energy consumption and computational complexity. In addition, cliff effects may occur if the packet loss rate (PLR) exceeds the correct capacity of channel coding [6].

Recently, compressive sensing (CS)-based image coding has been investigated as a convincing solution to the aforementioned problems. CS theory indicates that a compressible signal can be reconstructed from under-sampled measurements [7], [8]. Some benefits make CS a sensor-friendly compression method under the wireless visual sensor scenario. First, the CS-based coding scheme has a simple encoder since CS can sample and compress sparse or compressible signals in a single operation simultaneously. Second, the democracy property makes CS a robust image coding and transmission scheme [9]. Third, CS can increase the security level because it is under a low probability of successful attack by an adversary due to the need of estimating the measurement method [10]. However, the compression performance of the CS-based coding scheme is unsatisfactory. A large R-D performance gap exists between the CS-based coding and transmission schemes and traditional coding standards [11].

Some CS enhancement strategies have been explored to reduce this R-D gap at the cost of the encoder's complexity. For example, [12] performs the measurement in the discrete wavelet domain with a Gaussian matrix. More measurements are allocated to the low-frequency domain. However, such a sparse domain measurement increases the complexity of the encoder. In [13], motion detection is performed to identify the region of interest (ROI), and more bits are allocated to the ROI, which introduces a computation for extracting the ROI. In [14], a traditional source-channel coding compressed thumbnail is first transmitted to retrieve a reference similar image, and the residual image is coded and transmitted using CS-based transmission. Its R-D improvement highly relies on

Z. Chen, X. Hou, and X. Qian are with the School of Electronic and Information Engineering, Xi'an Jitaotong University, Xi'an, China, email: houxs@mail.xjtu.edu.cn.

C. Gong is with the School of Electronic and Information Engineering, University of Science and Technology of China, Hefei, China.

the image database for retrieval. The thumbnail procedure and additional source channel coding will increase the encoder's complexity.

In this paper, we propose a novel CS-based image coding and transmission scheme to keep the encoder complexity as low as possible without compromising the R-D performance. By using scrambled block compressive sampling (SBCS) with a separable sensing operator, progressive non-uniform quantization (PNQ) and progressive non-local low-rank reconstruction (NLR), the transmission can achieve simple encoding, good R-D performance and robustness against packet loss. The main contributions of this paper are summarized as follows:

First, we develop scrambled block compressed sampling with a separable sensing operator to reduce the encoder's complexity. Meanwhile, this random sampling method guarantees equal importance for each measurement, which makes the proposed coding scheme robust to packet loss.

Second, we propose a progressive non-uniform quantization method to improve the rate-distortion performance. This quantization method exploits the distribution and dependencies of the measurement results, which adds little computational burden to the encoder side.

Third, we develop an efficient progressive non-local low-rank CS reconstruction at the decoder side. Since the measurements are divided into the base layer and refinement layer, the reconstruction process is also divided into the two corresponding steps. This progressive non-local low-rank CS image restoration imparts the proposed coding scheme with higher R-D performance compared with other CS-based image coding methods.

The experimental results show that the proposed CS-based coding and transmission scheme has a low-complexity encoder (approximately one-third of the encoding time of CCSDS-IDC), high error resilience (stable reconstruction performance under different packet loss rates), and high R-D performance (higher PSNR than benchmark CS-based coding schemes).

The remainder of this paper is organized as follows. In Section II, we provide an overview of the CS-based transmission scheme and the related works. In Section III, we detail the encoder side, including the CS measurement method and quantization method. In Section IV, we detail the decoder side, including the proposed reconstruction method. The experimental results and performance analysis are provided in Section V. Finally, Section VI concludes this paper.

II. Overview of the CS-based Coding and Transmission Scheme

The CS-based coding and transmission scheme consists of encoder-side measurement and quantization and decoder-side reconstruction. These steps need to be delicately designed to achieve state-of-the-art coding efficiency with lower encoder computational complexity while still supporting error resilience.

The measurement step is related to the computational complexity of the CS-based coding scheme. Although a completely random sensing matrix offers optimal performance [7], it may suffer high computational complexity and low efficiency in practical implementations [15]. To reduce the measurement complexity, block compressive sampling (BCS) is proposed [16]. Furthermore, scrambled block compressive sampling (SBCS) has been proposed and theoretically proven to show sensing performance comparable to that of random sensing matrices for whole images [17], [18]. In [19], a 2-D separable sensing operator is proposed to reduce the measurement complexity. To reduce the encoder's complexity and guarantee the democracy property, we introduce image scrambled block compressive sampling with a separable sensing operator to obtain the CS measurements.

Quantization is crucial for improving the R-D performance in the CS-based coding scheme. In [12]–[14], uniform scalar quantization is employed in the CS-based coding and transmission scheme. In [20], a distortion model on the relationship between distortion, sampling ratio and quantization bit depth is proposed. In [21], a non-uniform quantization is designed according to the distribution of CS measurements. In [22], a progressive quantization scheme is proposed, which splits the CS measurements into the base layer and refinement layer and exploits the measurement dependencies at the decoder side. In this work, to enhance the R-D performance and keep the encoder simple, we propose a progressive non-uniform quantization (PNQ), which exploits the measurement distribution at the encoder side and the measurement dependencies at the decoder side.

An efficient reconstruction algorithm can enhance the R-D performance in the CS-based coding scheme. In BCS frames, BCS with smoothed projected Landweber (BCS-SPL) adopts the general paradigm of block-based random image sampling coupled with a projection-based reconstruction [23]. Multiscale BCS-SPL (MS-BCS-SPL) provides a variant of the original BCS-SPL reconstruction by deploying block-based CS sampling within the domain of a wavelet transform [24]. The endeavours in [25] improve the BCS reconstruction by imposing smoothness constraints between adjacent blocks. In other non-BCS frames, reconstruction algorithms based on tree-structured wavelet CS (TSW-CS) have been used in WVSN [12] [26]. The work in [27] provides a non-local low-rank CS reconstruction by exploiting the similar structure of nature images. In this work, we develop a progressive NLR reconstruction method to enhance the reconstructed image quality.

The diagram of the proposed CS-based image coding and transmission scheme is shown in Fig. 1. At the encoder side, the captured image is measured using scrambled block compressive sensing (SBCS) with a separable sensing operator. Then, the measurement results are quantized by non-uniform progressive quantization (PNQ). The quantized results are divided into the base layer and refinement layer, which are packaged and transmitted to the decoder side. At the decoder side, the proposed progressive non-local low-rank reconstruction (progressive NLR) method is utilized to recover the original image. Because the measurements are divided into the base layer and refinement layer, the reconstruction process is also divided corresponding to the two parts. In the following sections, we elaborate the above three steps, i.e., SBCS, PNQ and progressive NLR.

This article has been accepted for publication in a future issue of this journal, but has not been fully edited. Content may change prior to final publication. Citation information: DOI 10.1109/TMM.2017.2774004, IEEE Transactions on Multimedia

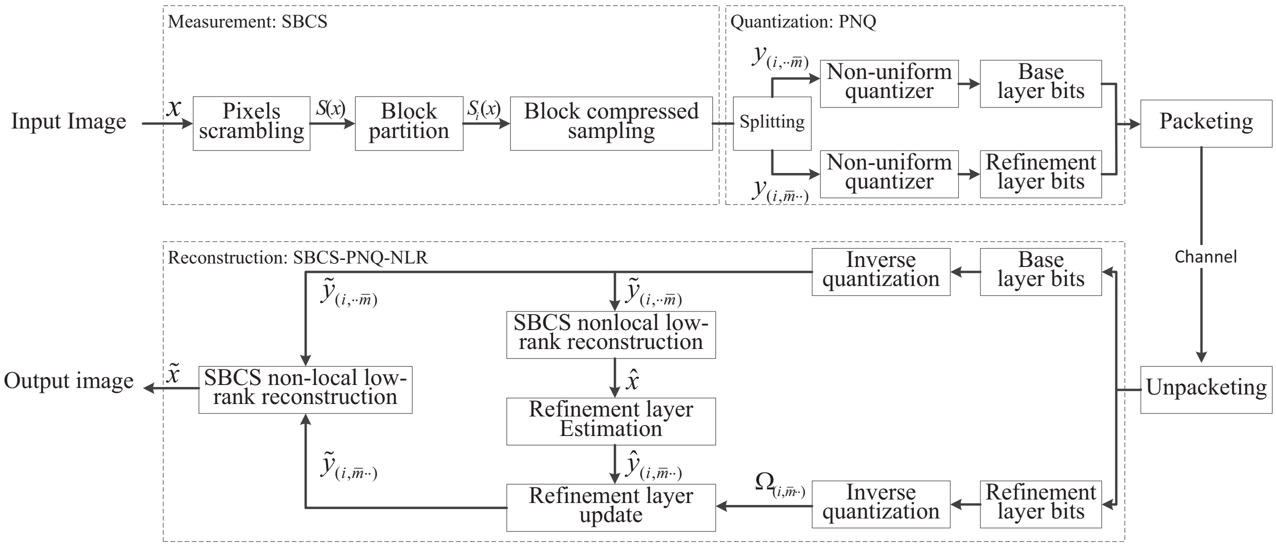

Fig. 1. Block diagram of the proposed CS-based image coding and transmission scheme.

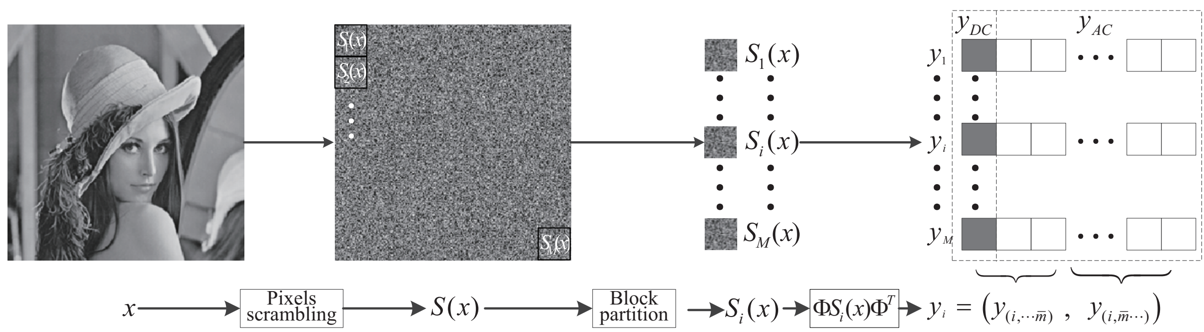

Fig. 2. The SBCS procedure.

III. Scrambled Block Compressive Sampling and Progressive Non-uniform Quantization

In this section, we elaborate the compressive sampling and quantization steps for the proposed CS-based coding and transmission scheme at the encoder side. The design criterion is to enhance the R-D performance while keeping the encoder as simple as possible.

A. Scrambled Block Compressive Sampling with Separable Sensing Operator

The procedure of the proposed measurement is shown in Fig. 2. We develop a measurement method using scrambled block compressive sampling with a separable sensing operator. In our model, we first reorder (i.e., scramble) the pixels of the whole image to spatially de-correlate the neighbouring blocks of pixels in a random manner [28]. Then, the scrambled image is divided into M non-overlapping sub-blocks with a size of $\sqrt{n}\times\sqrt{n}$, and the ith scrambled image block denoted as $S_i(x)$ is measured with a separable sensing operator

$$y_i = \Phi S_i(x)\Phi^{\mathrm{T}}, \tag{1}$$

where $y_i \in R^{\sqrt{m}\times\sqrt{m}}$ is the measurement result and $\Phi \in R^{\sqrt{m}\times\sqrt{n}}$ is a partial Hadamard matrix. We obtain Φ by selecting the first $\sqrt{m}$ rows of a $\sqrt{n}\times\sqrt{n}$ size Hadamard matrix.

This 2-D separable sensing operator described in Eq. (1) can be considered as a case of a traditional column-based CS measurement operator [29]. Suppose that $\bar{\Phi}$ can be decomposed into $\bar{\Phi} = (\Phi\otimes\Phi)$, where $\otimes$ is the Kronecker product operator. Eq. (1) can equivalently be represented as

$$vec(y_i) = \bar{\Phi} vec(S_i(x)), \tag{2}$$

where $vec(y_i)$ and $vec(S_i(x))$ are the row-ordered vectorizations of y_i and $S_i(x)$, respectively. Furthermore, Eq. (2) can characterize the block CS measurement, which can equivalently be expressed as a whole image CS measurement, i.e.,

$$\begin{bmatrix} vec(y_1) \\ \vdots \\ vec(y_M) \end{bmatrix} = (I_M \otimes \bar{\Phi}) \cdot \begin{bmatrix} vec(S_1(x)) \\ \vdots \\ vec(S_M(x)) \end{bmatrix}. \tag{3}$$

Considering that $S(x)$ is equivalent to multiplying $vec(x)$ by a matrix S, which is a random binary matrix that contains only one $'1'$ per row and column, we have

$$\begin{bmatrix} vec(S_1(x)) \\ \vdots \\ vec(S_M(x)) \end{bmatrix} = S \cdot vec(x). \tag{4}$$

Eq. (3) can further be represented as

$$vec(y) = (I_M \otimes \bar{\Phi}) \cdot S \cdot vec(x). \tag{5}$$

Thus, the equivalent measurement matrix of the proposed measurement method for the whole image can be represented as a structured random matrix $(I_M \otimes \bar{\Phi}) \cdot S$, which is nearly incoherent with almost all other orthonormal matrices and has theoretical sensing properties similar to those of completely random sensing matrices [18].

This SBCS with a separable Hadamard sensing operator presented in Eq. (1) requires $A_1 = (\sqrt{n}-1)\sqrt{m}\sqrt{n}+(\sqrt{n}-1)m$ add/sub operations, whereas the column-based sensing operator presented in Eq. (2) requires $A_2 = m(n-1)$ add/sub operations. Comparing A_1 and A_2, we have

$$\frac{A_1+m}{A_2+m} = \frac{1}{\sqrt{m}} + \frac{1}{\sqrt{n}} - \frac{1}{\sqrt{m}\sqrt{n}} \leq 1, \tag{6}$$

which shows that $A_1 \leq A_2$. Thus, this separable sensing operator has a lower computational complexity compared with the traditional column-based sensing operator.

B. Progressive Non-uniform Quantization

In this subsection, we first exploit the dependencies among the measurements by utilizing the progressive quantization strategy. To further improve the R-D performance, we subsequently design a non-uniform quantizer based on the measurement distribution. The proposed progressive non-uniform quantizer increases the R-D performance while having low computational complexity at the encoder side.

1) Progressive Quantization: Suppose that $y_{(i,j)}$ is the jth measurement value of the ith block for SBCS measurements. Conventionally, each measurement $y_{(i,j)}$ is quantized and transmitted in fixed-length bits. However, this strategy disregards the dependencies among CS measurements. To improve the R-D performance, we exploit the correlation for SBCS measurements by adopting a progressive quantization strategy.

For the progressive quantization strategy, the measurement values of the ith block are divided into base layer $y_{(i,\cdot\cdot\bar{m})}$ and refinement layer $y_{(i,\bar{m}\cdot\cdot)}$, where $y_{(i,\cdot\cdot\bar{m})}$ consists of the first $\bar{m}$ measurements and $y_{(i,\bar{m}\cdot\cdot)}$ consists of the remaining $m-\bar{m}$ measurements. To obtain $y_{(i,\cdot\cdot\bar{m})}$ and $y_{(i,\bar{m}\cdot\cdot)}$, the partial Hadamard measurement matrix Φ in Eq. (1) is regarded as being composed of two matrices, that is,

$$\Phi = \begin{bmatrix} \Phi_{\cdot\cdot\bar{m}} \\ \Phi_{\bar{m}\cdot\cdot} \end{bmatrix}. \tag{7}$$

By substituting Eq. (7) into Eq. (1), the SBCS measurement procedure can be rewritten as follows:

$$\begin{bmatrix} y_{(i,\cdot\cdot\bar{m})} \ y_{(i,\bar{m}\cdot\cdot)} \end{bmatrix} = \Phi S_i(x) \begin{bmatrix} \Phi^{\mathrm{T}}_{\cdot\cdot\bar{m}} \ \Phi^{\mathrm{T}}_{\bar{m}\cdot\cdot} \end{bmatrix}. \tag{8}$$

In this way, the base layer $y_{(i,\cdot\cdot\bar{m})}$ and refinement layer $y_{(i,\bar{m}\cdot\cdot)}$ can respectively be obtained via the following two partial Hadamard projections:

$$y_{(i,\cdot\cdot\bar{m})} = \Phi S_i(x) \Phi^{\mathrm{T}}_{\cdot\cdot\bar{m}}\ , \tag{9}$$

$$y_{(i,\bar{m}\cdot\cdot)} = \Phi S_i(x) \Phi^{\mathrm{T}}_{\bar{m}\cdot\cdot}\ . \tag{10}$$

Consider the CS decoder that can recover an initial estimated result $S_i(\hat{x})$ by using the first $\bar{m}$ CS measurements $y_{(i,\cdot\cdot\bar{m})}$. It can generate an approximate refinement layer $y_{(i,\bar{m}\cdot\cdot)}$ by $\Phi S_i(\hat{x})\Phi^{\mathrm{T}}_{\bar{m}\cdot\cdot}$ at the decoder side, which means that $y_{(i,\cdot\cdot\bar{m})}$ has side information on $y_{(i,\bar{m}\cdot\cdot)}$ [30].

In the proposed CS-based coding and transmission scheme, for each scrambled block measurement, only the first $\bar{m}$ SBCS measurement values $y_{(i,\cdot\cdot\bar{m})}$ (base layer) are transmitted with a total of B bits, while the remaining $m-\bar{m}$ SBCS measurement values $y_{(i,\bar{m}\cdot\cdot)}$ (refinement layer) are transmitted with only the b least significant bits. The dropped $B-b$ most significant bits for $y_{(i,\bar{m}\cdot\cdot)}$ can be predicted from $\Phi S_i(\hat{x})\Phi^{\mathrm{T}}_{\bar{m}\cdot\cdot}$ at the decoder side. In this way, the encoder saves $(m-\bar{m})(B-b)$ bits for each measurement block compared with fixed-length bit code, which can improve the R-D performance.

2) Non-uniform Quantization: In [22], the base layer and refinement layer are sent to the uniform quantizer. This uniform quantization does not utilize the statistical characteristics of the measurement values and suffers from lower compression efficiency. Thus, we select non-uniform quantization levels and decision levels based on the distribution of the SBCS measurement values, which can reduce the average distortion for a fixed quantization bit depth.

The scrambled image $S(x)$ is divided into M blocks and compressed into $M \times m$ measurement values using compressive sampling, which is further divided into $y_{(i,\cdot\cdot\bar{m})}$ and $y_{(i,\bar{m}\cdot\cdot)}$ as shown in Fig. 2. Since the pixels in the scrambled image block are identically and independently distributed, the SBCS measurement values $y_{(i,j)}$ follow a Gaussian distribution based on central limit theory [31]. Assuming that $S(x)$ satisfies a Gaussian distribution with mean μ and variance σ^2, we have that $\frac{y_{DC}}{n} \sim \mathbf{N}(\mu, \frac{\sigma^2}{n})$ and $\frac{y_{AC}}{n} \sim \mathbf{N}(0, \frac{\sigma^2}{n})$, where the DC part y_{DC} consists of the first column of y and the AC part y_{AC} consists of the remaining columns.

The DC part and AC part are first normalized to a standard Gaussian distribution and then processed by the non-uniform quantizer. The non-uniform quantizer is pre-trained offline using the Lloyd-Max design [32] for the standard Gaussian distribution. For non-uniform quantization, there are more quantization levels around the mean point compared with uniform quantization according to the probability distribution of SBCS measurements. By using table lookups, the base layer and refinement layer can be non-uniformly quantized with low computational cost.

IV. Progressive Non-local Low-Rank CS Reconstruction for SBCS and PNQ

In this section, we elaborate the reconstruction algorithm at the decoder side. A progressive non-local low-rank reconstruction algorithm at the decoder side, which exploits the self-similarity of image and measurement dependencies, is designed to reconstruct the image from the SBCS and PNQ outputs. This reconstruction algorithm will improve the R-D performance without increasing the encoder's complexity.

A. Non-local Low-Rank Reconstruction

Repetitive similar structures exist in an image, such as smooth structure, texture structure, and edge structure. Denote

This article has been accepted for publication in a future issue of this journal, but has not been fully edited. Content may change prior to final publication. Citation information: DOI 10.1109/TMM.2017.2774004, IEEE Transactions on Multimedia

$p_{i,j}(x)$ as the jth similar patch of an exemplar patch $p_i(x)$ in a search window of size w. The top q patches under a mean squared error (MSE) criterion are vectorized and grouped to form $P_i(x) = [p_{i,1}(x), p_{i,2}(x), ...p_{i,q}(x)]$, as shown in Fig. 3. Since the columns of $P_i(x)$ are similar with each other, we can assume that $P_i(x)$ is a low-rank matrix [33]. However, $P_i(x)$ may be corrupted by noise, which could lead to deviation from the desirable low-rank constraint. To obtain an approximate low-rank solution to $P_i(x)$, the nuclear norm (sum of the singular values) can be used as a convex surrogate of the rank [27].

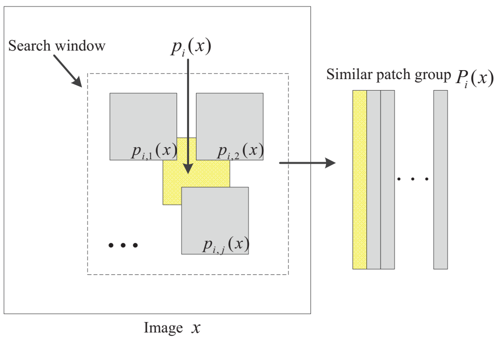

Fig. 3. Illustration of similar patch search.

We thus formulate the CS reconstruction problem as the low-rank matrix approximation problem with measurement and nuclear norm constraints, which is formulated as follows:

$$\begin{cases} \arg\min\limits_{x} & \sum\limits_{i=1}^{N} \| P_i(x) \|_*, \\ s.t. & y_i = \Phi S_i(x) \Phi^{\mathrm{T}},\ i = 1, ..., M, \end{cases} \tag{11}$$

where N is the number of similar patch groups in the entire image and $\| \|_*$ is the nuclear norm operator. Using the nuclear norm, the rank minimization problem can be efficiently solved using the singular value thresholding (SVT) technique [34].

To solve Eq. (11), we take two steps to optimize $\| P_i(x) \|_*$ and x alternatively. The kth iterations of the reconstructed image for *Step 1* and *Step 2* are denoted as $x^{(2k+1)}$ and $x^{(2k)}$, respectively, and the initial $x^{(0)}$ is reconstructed using BCS-SPL [23].

Step 1 (Low-Rank Approximation): We first find $P_i(x^{(2k)})$ by grouping similar patches in $x^{(2k)}$. Let $U\Sigma V^{\mathrm{T}}$ be the singular value decomposition of the matrix $P_i(x^{(2k)})$, where Σ is the diagonal matrix composed of σ_r, the rth singular values of $P_i(x^{(2k)})$. The low-rank approximation of $P_i(x^{(2k)})$ is obtained using the soft-thresholding method

$$P_i(x^{(2k+1)}) = U\rho(\Sigma)V^{\mathrm{T}}, \tag{12}$$

where ρ is a diagonal operator defined as

$$\rho(\Sigma) = \max(\Sigma - \tau diag(\omega), 0). \tag{13}$$

The soft-threshold value is determined by τ and ω, where τ is a preset coefficient to adjust the threshold and ω is a weighted parameter to adapt the singular value Σ. The rth value of ω is defined as $\omega_r = 1/(\sigma_r + \varepsilon)$ [27], where ε denotes a small constant value. From Eq. (12), we can obtain a set of new low-rank patches $P_i(x^{(2k+1)})$ and output the reconstructed image $x^{(2k+1)}$ for *Step 1*.

Step 2 (SBCS Measurement Constraint): To guarantee that the reconstructed image $x^{(2k+1)}$ from *Step 1* satisfies the SBCS measurement constraint $y_i = \Phi S_i(x)\Phi^{\mathrm{T}}$, we update the scrambled image block $S_i(x^{(2k+1)})$ by

$$S_i(x^{(2k+2)}) = S_i(x^{(2k+1)}) + \Phi^{+}(y_i - \Phi S_i(x^{(2k+1)})\Phi^{\mathrm{T}})(\Phi^{+})^{\mathrm{T}}, \tag{14}$$

where Φ^{+} is the pseudo-inverse of Φ. Since Φ is a partial Hadamard matrix, we have $\Phi^{+} = \Phi^{\mathrm{T}}(\Phi\Phi^{\mathrm{T}})^{-1} = \frac{1}{\sqrt{n}}\Phi^{\mathrm{T}}$. Thus, Eq. (14) can be rewritten as

$$S_i(x^{(2k+2)}) = S_i(x^{(2k+1)}) + \frac{1}{n}\Phi^{\mathrm{T}}(y_i - \Phi S_i(x^{(2k+1)})\Phi^{\mathrm{T}})\Phi. \tag{15}$$

By tiling each scrambled image block $S_i(x^{(2k+2)})$, we obtain the updated scrambled image $S(x^{(2k+2)})$. Let $S^{-1}(\cdot)$ denote the inverse operator of $S(\cdot)$, which restores the order of the pixels. We output the reconstructed image $x^{(2k+2)}$ for *Step 2* by

$$x^{(2k+2)} = S^{-1}(S(x^{(2k+2)})). \tag{16}$$

Through updating $x^{(k)}$ based on *Step 1* and *Step 2* iteratively, we can find the low-rank approximation solution x for Eq. (11).

B. Progressive Non-local Low-Rank Reconstruction

For the progressive strategy, the decoder receives all B bits per measurement for the base layer and only the least significant b bits per measurement for the refinement layer. By performing inverse non-uniform quantization, we obtain $\tilde{y}_{(i,\cdot\cdot\bar{m})}$ for the base layer and a set $\Omega_{(i,\bar{m}\cdot\cdot)}$ that contains possible values of $\tilde{y}_{(i,\bar{m}\cdot\cdot)}$ with the same insignificant b bits as those received for the refinement layer. Thus, the low-rank matrix problem presented in Eq. (11) is modified for the progressive strategy, formulated as follows:

$$\begin{cases} \arg\min\limits_{x} & \sum\limits_{i=1}^{N} \| P_i(x) \|_* \\ & \tilde{y}_{(i,\cdot\cdot\bar{m})} = \Phi S_i(x)\Phi^{\mathrm{T}}_{(i,\cdot\cdot\bar{m})}, \\ s.t. & \tilde{y}_{(i,\bar{m}\cdot\cdot)} = \Phi S_i(x)\Phi^{\mathrm{T}}_{(i,\bar{m}\cdot\cdot)}, \\ & \tilde{y}_{(i,\bar{m}\cdot\cdot)} \in \Omega_{(i,\bar{m}\cdot\cdot)},\ i = 1, ..., M. \end{cases} \tag{17}$$

To find the solution to this problem, we first reconstruct an approximation of the image with the base layer data, and then we estimate and update the refinement layer. Finally, we find the final solution by solving a low-rank matrix problem with the base layer and refinement layer SBCS measurement constraint.

1) Reconstruction with the Base Layer: We first reconstruct an approximated $\hat{x}$ using base layer data $\tilde{y}_{(i,\cdot\cdot\bar{m})}$. The reconstruction problem is formulated as

$$\begin{cases} \arg\min\limits_{\hat{x}} & \sum\limits_{i=1}^{N} \| P_i(\hat{x}) \|_* \\ s.t. & \tilde{y}_{(i,\cdot\cdot\bar{m})} = \Phi S_i(\hat{x})\Phi^{\mathrm{T}}_{\cdot\cdot\bar{m}}, i = 1, ..., M. \end{cases} \tag{18}$$

This article has been accepted for publication in a future issue of this journal, but has not been fully edited. Content may change prior to final publication. Citation information: DOI 10.1109/TMM.2017.2774004, IEEE Transactions on Multimedia

We find a solution $\hat{x}$ to Eq. (18) using the method proposed in Section IV-A except that the related Eq. (15) is changed to the following:

$$S_i(x) = S_i(x) + \frac{1}{n}\Phi^{\mathrm{T}}(\tilde{y}_{(i,\cdot\cdot\bar{m})} - \Phi S_i(x)\Phi^{\mathrm{T}}_{\cdot\cdot\bar{m}})\Phi_{\cdot\cdot\bar{m}}. \quad (19)$$

This base layer reconstruction image $\hat{x}$ is used to obtain an estimated refinement layer $\hat{y}_{(i,\bar{m}\cdot\cdot)}$.

2) Estimate and Update the Refinement Layer: After obtaining the approximate reconstruction $\hat{x}$, we estimate the refinement layer $y_{(i,\bar{m}\cdot\cdot)}$ by

$$\hat{y}_{(i,\bar{m}\cdot\cdot)} = \Phi S_i(\hat{x})\Phi^{\mathrm{T}}_{\bar{m}\cdot\cdot}. \quad (20)$$

Then, we adopt the maximum a posteriori probability (MAP) estimator to update the estimation $\tilde{y}_{(i,\bar{m}\cdot\cdot)}$ by exploiting the received b least significant bits of $y_{(i,m\cdot\cdot)}$, i.e.,

$$\begin{aligned}\tilde{y}_{(i,\bar{m}\cdot\cdot)} &= \underset{\tilde{y}_{(i,\bar{m}\cdot\cdot)}\in\Omega_{(i,\bar{m}\cdot\cdot)}}{\arg\max}\; p(\tilde{y}_{(i,\bar{m}\cdot\cdot)}|\hat{y}_{(i,\bar{m}\cdot\cdot)}) \\ &= \underset{\tilde{y}_{(i,\bar{m}\cdot\cdot)}\in\Omega_{(i,\bar{m}\cdot\cdot)}}{\arg\min}\; \parallel \tilde{y}_{(i,\bar{m}\cdot\cdot)} - \hat{y}_{(i,\bar{m}\cdot\cdot)} \parallel,\end{aligned} \quad (21)$$

where $\Omega_{(i,\bar{m}\cdot\cdot)}$ is the set of possible $\tilde{y}_{(i,\bar{m}\cdot\cdot)}$ with the same quantized b least significant bits of the received refinement layer part. In this way, we update the refinement layer from $\hat{y}_{(i,\bar{m}\cdot\cdot)}$ to $\tilde{y}_{(i,\bar{m}\cdot\cdot)}$.

3) Reconstruction with Base and Refinement Layers: Note that we have obtained the base layer $\tilde{y}_{(i,\cdot\cdot\bar{m})}$ and refinement layer $\tilde{y}_{(i,\bar{m}\cdot\cdot)}$. The problem in Eq. (17) is simplified to a low-rank matrix problem with the following base layer and refinement layer SBCS measurement constraints:

$$\begin{cases} \underset{x}{\arg\min} & \sum_{i=1}^{N} \parallel P_i(x) \parallel_* \\ s.t. & \tilde{y}_{(i,\cdot\cdot\bar{m})} = \Phi S_i(x)\Phi^{\mathrm{T}}_{(i,\cdot\cdot\bar{m})}, \\ & \tilde{y}_{(i,\bar{m}\cdot\cdot)} = \Phi S_i(x)\Phi^{\mathrm{T}}_{(i,\bar{m}\cdot\cdot)}, i = 1, ..., M, \end{cases} \quad (22)$$

which has one more $\tilde{y}_{(i,m\cdot\cdot)}$ constraint than Eq. (18). The solution is given by

$$\begin{aligned} S_i(x) = S_i(x) &+ \frac{1}{n}\Phi^{\mathrm{T}}(\tilde{y}_{(i,\cdot\cdot\bar{m})} - \Phi S_i(x)\Phi^{\mathrm{T}}_{\cdot\cdot\bar{m}})\Phi_{\cdot\cdot\bar{m}} \\ &+ \frac{1}{n}\Phi^{\mathrm{T}}(\tilde{y}_{(i,\bar{m}\cdot\cdot)} - \Phi S_i(x)\Phi^{\mathrm{T}}_{\bar{m}\cdot\cdot})\Phi_{\bar{m}\cdot\cdot} \end{aligned} \quad (23)$$

Algorithm 1 provides the pseudo-code for the proposed SBCS-PNQ-NLR scheme.

In Algorithm 1, the base layer data are involved in all iterations, whereas the refinement layer data are only involved in reconstruction after K_0 ($K_0 = 200$ in our implementation) iterations. To better show the convergence of Algorithm 1, we present the average PSNR obtained from the CS reconstruction for the 48 test images with respect to iterations with different compression rates. We can observe that the proposed method gradually converges in two steps, which correspond to Sec. IV-B-1 (reconstruction with base layer) and Sec. IV-B-3 (reconstruction with base and refinement layer). The progressive NLR has a better CS reconstruction compared with the original NLR [27].

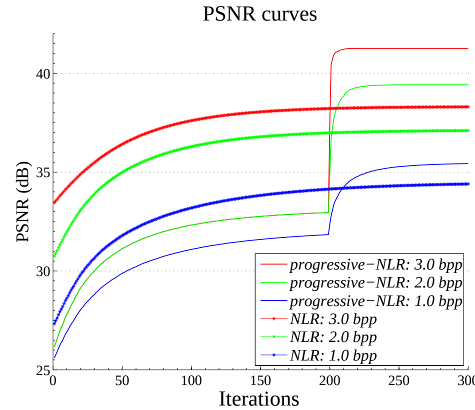

Fig. 4. Average PSNR of the CS recovery for 48 test images with respect to the iterations. Progressive-NLR denotes the proposed CS method. NLR denotes the CS method in [27].

Algorithm 1 The SBCS-PNQ-NLR Algorithm

Input:
- The base layer bits and refinement layer bits

Output:
- A reconstruction $\tilde{x}$ of the original image x

Initialization:

(a) Obtain $\tilde{y}_{(i,\cdot\cdot\bar{m})}$ from the received base layer bits
(b) Obtain $\Omega_{(i,\bar{m}\cdot\cdot)}$ from the refinement layer bits
(c) Estimate an initial image $x^{(0)}$ from $\tilde{y}_{(i,\cdot\cdot\bar{m})}$ using a block-based CS recovery method (e.g., BCS-SPL)

for $k = 0, 1, ..., K$ **do**
(I) **Step 1** (low-rank approximation):
  for $i = 1, 2, ..., N$ **do**
    Group a set of similar patches $P_i(x^{2k})$
    Singular value decomposition of $P_i(x^{2k})$
    Calculate $P_i(x^{(2k+1)})$ via Eq. (12)
  end for
  Output $x^{(2k+1)}$ with $P_i(x^{(2k+1)})$
(II) **Step 2** (SBCS measurement constraint):
  if $k <= K_0$ (base layer constraint):
    for $i = 1, 2, ..., M$ **do**
      Compute $S_i(x^{(2k+2)})$ via Eq. (19)
    end for
    Output $x^{(2k+2)}$ via Eq. (16)
  else (base and refinement layer constraint):
    Take $x^{(2k+1)}$ as $\hat{x}$
    for $i = 1, 2, ..., M$ **do**
      Estimate $\hat{y}_{(i,\bar{m}\cdot\cdot)}$ via Eq. (20)
      Update $\hat{y}_{(i,\bar{m}\cdot\cdot)}$ into $\tilde{y}_{(i,\bar{m}\cdot\cdot)}$ via Eq. (21)
      Compute $S_i(x^{(2k+2)})$ via Eq. (23)
    end for
    Update $x^{(2k+2)}$ via Eq. (16)
  end if
end for
Return $\tilde{x} = x^{(2K+2)}$

This article has been accepted for publication in a future issue of this journal, but has not been fully edited. Content may change prior to final publication. Citation information: DOI 10.1109/TMM.2017.2774004, IEEE Transactions on Multimedia

Fig. 5. The test images for experiments. From left to right, the first eight images are denoted as Barbara, Lena, Monarch, Peppers, Boats, Parrots, Foreman and House.

(a) (b) (c) (d) (e)

Fig. 6. Reconstructed Barbara with 0.5 bpp. (a) Original image, (b) proposed SBCS-PNQ-NLR (30.13 dB) recovery, (c) BCS-SPL (22.84 dB) recovery, (d) MS-BCS-SPL (23.65 dB) recovery, and (e) TSW-CS (23.41 dB) recovery.

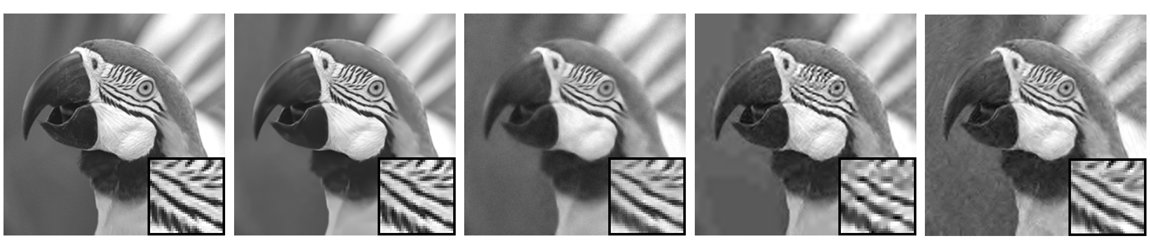

(a) (b) (c) (d) (e)

Fig. 7. Reconstructed Parrots with 1.0 bpp. (a) Original image, (b) proposed SBCS-PNQ-NLR (36.13 dB) recovery, (c) BCS-SPL (29.31 dB) recovery, (d) MS-BCS-SPL (29.15 dB) recovery, and (e) TSW-CS (29.14 dB) recovery.

V. Experimental Results and Analysis

For the proposed SBCS-PNQ-NLR scheme, each test image is compressed by SBCS with a separable sensing operator and PNQ at the encoder side and reconstructed by progressive NLR at the decoder side.

In addition to R-D performance, the encoder complexity and packet loss robustness should be considered in the WVSN scenario. Hence, we first compare the R-D performance of the proposed SBCS-PNQ-NLR with other CS-based coding schemes and conventional source coding schemes to show the improvement in efficiency of SBCS-PNQ-NLR. Then, we compare the robustness of the proposed SBCS-PNQ-NLR and source-channel coding schemes under packet loss channels. Subsequently, we test the running time for the encoder of the proposed method. Finally, we discuss the main parameter of the proposed scheme, i.e., bit allocation between the base and refinement layers in PNQ, and we show the improvement in performance of PNQ.

For the SBCS with a separable sensing operator, a 16×16 codeblock size is set, and a corresponding partial Hadamard matrix is chosen as the separable measurement matrix. Each CS measurement is quantized into 5 bits. For the base layer data, all 5 bits are transmitted, whereas for the refinement layer data, only the least 3 significant bits are transmitted. We take the compression ratio by adjusting the sample rate. Forty-eight standard 256×256 greyscale images with 8 bpp (bits per pixel), as shown in Fig. 5, are used to verify the validity. The first 24 images are from the UGR Computer Vision Group image repository [35], and the left images are from ImageNet [36]. For the experiments, we present the results of the first eight images and the average results of all forty-eight test images.

A. R-D Efficiency Comparison

1) Comparison with CS-based Coding Schemes: In this part, we compare SBCS-PNQ-NLR with the benchmark CS-based approaches, which are MS-BCS-SPL, BCS-SPL and TSW-CS, because they have been reported to be applied for image coding and transmission. Note that the standard uniform quantization is chosen for TSW-CS, MS-BCS-SPL and BCS-SPL, and there is no entropy coding for any CS-based schemes. The PSNR results are presented in TABLE I, which are encoded from 0.5 bpp to 3.0 bpp. The reconstruction PSNR results of SBCS-PNQ-NLR obtain significant enhancement compared with other CS-based schemes. To evaluate the reconstruction quality from the subjective perspective, the reconstructed images are shown in Figs. 6 and 7. It is apparent that the proposed SBCS-PNQ-NLR achieves the best visual quality among the competing CS-based coding schemes.

The R-D performance can be justified via the following three aspects. First, the non-local low-rank reconstruction algorithm exploits the group sparsity of similar patches, which outperforms the existing state-of-the-art CS recovery techniques [27]. Second, the progressive quantization strategy enables the CS decoder to exploit hidden correlations among the CS measurements [22]. Third, the non-uniform quantization strategy utilizes the distribution of CS measurements [31]. The impact of quantization will be tested and discussed in Section V-D below.

2) Comparison with Conventional Source Coding Schemes: CCSDS-IDC, JPEG2000 and HEVC-intra are three typical image data compression algorithms that are widely used as source coding methods. Among the three traditional source coding methods, CCSDS-IDC is proposed for space image compression on board. JPEG2000 is more complicated than CCSDS-IDC, and HEVC-intra is the most complicated.

We compare the R-D performance of the proposed SBCS-PNQ-NLR scheme with the above sophisticated image data compression algorithms. To simplify the encoder, we add no entropy coder after the quantization for SBCS-PNQ-NLR. TABLE II shows the bit rate and PSNR obtained on test

TABLE I
PSNR(dB) COMPARISON WITH OTHER CS-BASED CODING SCHEMES

Image	Method	bpp					
		0.5	1.0	1.5	2.0	2.5	3.0
Barbara	**SBCS-PNQ-NLR**	**30.13**	**35.34**	**37.62**	**39.31**	**40.56**	**41.59**
	BCS-SPL	22.84	23.78	24.70	25.73	27.05	28.52
	MS-BCS-SPL	23.65	25.02	26.30	26.96	27.18	27.26
	TSW-CS	23.41	25.92	27.79	30.37	31.70	32.89
Lena	**SBCS-PNQ-NLR**	**30.68**	**35.47**	**38.05**	**40.10**	**41.54**	**42.62**
	BCS-SPL	25.01	27.31	28.87	30.36	31.90	33.10
	MS-BCS-SPL	27.64	30.33	32.38	33.05	33.99	34.29
	TSW-CS	24.55	28.24	29.34	31.93	33.07	34.36
Monarch	**SBCS-PNQ-NLR**	**28.84**	**33.96**	**36.71**	**38.85**	**40.10**	**41.01**
	BCS-SPL	22.00	24.71	26.50	28.21	29.85	31.30
	MS-BCS-SPL	24.97	28.53	30.72	31.54	32.71	33.15
	TSW-CS	22.03	25.38	27.90	30.03	31.27	32.95
Peppers	**SBCS-PNQ-NLR**	**30.13**	**34.46**	**36.42**	**38.11**	**39.52**	**40.78**
	BCS-SPL	24.42	27.06	28.87	30.35	31.65	32.79
	MS-BCS-SPL	26.04	28.77	30.83	32.67	32.75	33.11
	TSW-CS	22.77	25.30	28.90	31.09	32.64	33.64
Boats	**SBCS-PNQ-NLR**	**29.97**	**35.05**	**37.81**	**39.58**	**40.96**	**42.16**
	BCS-SPL	24.25	26.26	27.72	29.05	30.30	31.54
	MS-BCS-SPL	26.91	29.66	31.40	31.34	32.06	32.25
	TSW-CS	24.33	27.50	29.37	31.24	32.79	33.77
Parrots	**SBCS-PNQ-NLR**	**32.13**	**36.13**	**38.09**	**39.60**	**40.73**	**41.44**
	BCS-SPL	25.77	29.31	31.18	32.58	33.66	34.46
	MS-BCS-SPL	26.62	29.15	31.59	32.43	33.86	34.29
	TSW-CS	24.83	29.14	31.48	33.45	34.60	35.08
Foreman	**SBCS-PNQ-NLR**	**35.33**	**38.20**	**39.80**	**41.11**	**42.09**	**42.65**
	BCS-SPL	29.68	32.25	33.71	34.87	35.68	36.27
	MS-BCS-SPL	31.98	34.40	37.35	37.31	39.12	39.76
	TSW-CS	29.44	33.08	34.69	35.74	37.07	37.76
House	**SBCS-PNQ-NLR**	**34.42**	**37.54**	**39.45**	**40.94**	**42.24**	**43.28**
	BCS-SPL	27.51	30.31	32.09	33.41	34.53	35.48
	MS-BCS-SPL	29.15	31.93	33.87	34.74	36.15	36.65
	TSW-CS	26.24	30.23	32.58	34.21	34.91	35.71
Average	**SBCS-PNQ-NLR**	**30.94**	**35.43**	**37.77**	**39.42**	**40.54**	**41.26**
	BCS-SPL	24.85	27.28	28.99	30.52	31.90	33.23
	MS-BCS-SPL	27.03	29.56	31.05	31.26	32.93	34.30
	TSW-CS	22.95	26.40	29.30	31.55	33.31	34.47

TABLE II
PSNR (dB) COMPARISON WITH TRADITIONAL SOURCE CODING METHODS

Image	Method	bpp					
		0.50	1.00	1.50	2.00	2.50	3.00
Barbara	**SBCS-PNQ-NLR**	30.13	35.34	37.62	39.31	40.56	41.59
	CCSDS-IDC	30.10	34.76	38.49	40.93	43.18	44.86
	JPEG2000	31.56	36.74	40.36	43.12	45.56	47.81
	HEVC-intra	33.55	38.93	42.00	44.62	47.06	49.18
Lena	**SBCS-PNQ-NLR**	30.68	35.47	38.05	40.10	41.54	42.62
	CCSDS-IDC	32.52	37.84	40.93	43.88	45.58	48.44
	JPEG2000	33.32	39.13	42.75	45.58	47.96	50.25
	HEVC-intra	35.79	41.09	44.79	47.41	50.19	52.44
Monarch	**SBCS-PNQ-NLR**	28.84	33.96	36.71	38.85	40.10	41.01
	CCSDS-IDC	29.21	34.72	38.73	41.14	43.73	45.32
	JPEG2000	29.84	35.62	39.92	43.36	45.70	47.99
	HEVC-intra	33.33	39.37	42.98	45.48	48.23	50.48
Peppers	**SBCS-PNQ-NLR**	30.13	34.46	36.42	38.11	39.52	40.78
	CCSDS-IDC	32.13	36.22	38.95	41.09	42.97	44.57
	JPEG2000	32.56	37.40	40.32	42.77	45.06	47.15
	HEVC-intra	35.11	39.20	42.14	44.38	47.25	49.85
Boats	**SBCS-PNQ-NLR**	29.97	35.05	37.81	39.58	40.96	42.16
	CCSDS-IDC	31.56	36.60	39.70	42.36	43.95	45.84
	JPEG2000	32.88	38.05	41.44	44.15	46.35	48.90
	HEVC-intra	35.39	40.33	43.32	45.94	48.52	51.29
Parrots	**SBCS-PNQ-NLR**	32.13	36.13	38.09	39.60	40.73	41.44
	CCSDS-IDC	35.40	39.68	42.18	44.01	45.99	48.59
	JPEG2000	35.85	40.81	43.87	45.99	48.35	50.67
	HEVC-intra	37.37	42.35	45.24	48.09	50.44	53.40
Foreman	**SBCS-PNQ-NLR**	35.33	38.20	39.80	41.11	42.09	42.65
	CCSDS-IDC	37.16	40.98	44.42	45.97	49.12	50.61
	JPEG2000	38.21	42.65	46.07	48.79	50.98	53.22
	HEVC-intra	40.88	45.05	48.62	50.75	53.48	56.40
House	**SBCS-PNQ-NLR**	34.42	37.54	39.45	40.94	42.24	43.28
	CCSDS-IDC	35.60	39.51	42.08	44.32	46.31	48.70
	JPEG2000	36.12	40.97	44.30	46.81	49.08	51.19
	HEVC-intra	39.49	43.17	46.27	49.01	51.23	54.28
Average	**SBCS-PNQ-NLR**	30.94	35.43	37.77	39.42	40.54	41.26
	CCSDS-IDC	32.39	37.34	40.57	43.01	45.09	47.08
	JPEG2000	33.80	39.09	42.68	45.52	47.98	50.27
	HEVC-intra	36.80	41.66	45.08	47.99	50.88	54.26

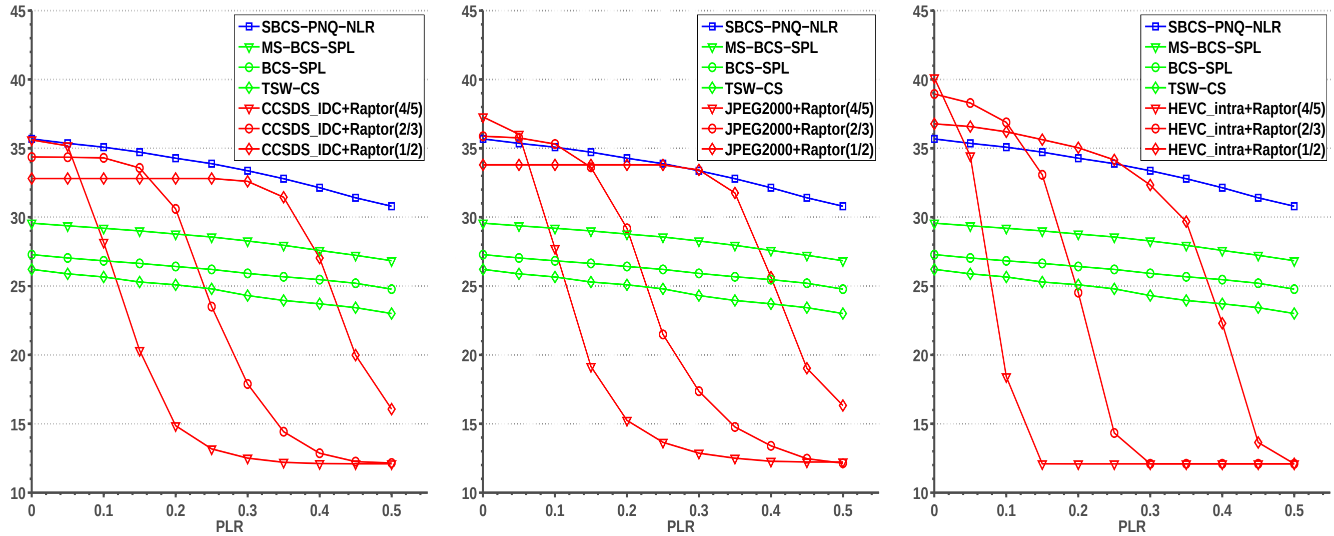

(a) (b) (c)

Fig. 8. The average PSNR of CS-based coding and transmission schemes and traditional source channel coding encoded at 1.0 bpp under various PLRs: (a) comparison with CCSDS-IDC with Raptor codes, (b) comparison with JPEG2000 with Raptor codes, and (c) comparison with HEVC-intra with Raptor codes.

images. The test images are encoded at 0.5 bpp, 1 bpp, 1.5 bpp, 2.0 bpp, 2.5 bpp and 3.0 bpp. The average PSNR result of the proposed SBCS-PNQ-NLR is approximately 1.5 dB lower than the CCSDS-IDC for 0.5 bpp compression. However, in the packet loss condition, the proposed SBCS-PNQ-NLR obtains higher or similar performance compared with the traditional source-channel coding schemes, as shown in subsection V-B. Moreover, the CS coding and transmission scheme is simple and efficient on the encoder side, which is amenable for implementation on visual sensors. The traditional source coding achieves higher compression efficiency at the expense of higher encoder computational complexity, which is shown in subsection V-C.

B. Packet Loss Robustness Comparison

In this part, we simulate the transmission of compressed images under packet loss conditions to evaluate the robustness. For conventional source-channel coding schemes, a source coding codestream is transmitted with certain channel coding redundancy. We take CCSDS-IDC, JPEG2000, and HEVC-intra for source coding and Raptor codes for channel coding. Note that Raptor code serves as a good candidate for the channels with packet loss, which has been integrated into IP Datacast services by DVB [37] and standardized by 3GPP in MBMS services [38].

We test the R-D performance of the proposed SBCS-PNQ-NLR scheme and three traditional source coding schemes under different PLRs at a 1.0 bpp compression ratio. The bitstreams of the proposed SBCS-PNQ-NLR scheme for 1.0 bpp are grouped into 164 packets, i.e., each packet consists of 400 bits for compression data, with 99 packets for the base layer and 65 packets for the refinement layer. Consider the fixed-rate Raptor code of rate $\frac{s}{r}$, where blocks of s source coding bits are encoded into codewords of r bits. Three fixed-rate $\frac{s}{r}$ are selected: $4/5$, $2/3$, and $1/2$. Random packet loss is assumed, and the simulations are repeated 200 times. The average reconstructed PSNRs of the forty-eight tested images under channel packet loss are reported in Fig. 8. This figure shows that the proposed SBCS-PNQ-NLR scheme outperforms or matches the CCSDS-IDC with Raptor codes and JPEG2000 with Raptor codes in most packet loss rates. Although more redundancy could enhance the robustness to packet loss, it reduces the R-D performance. For traditional source coding schemes with fixed channel coding redundancy, if a receiver is unable to collect sufficient coded symbols, then the received packets would not be decoded. In such a case, the overall recovery quality would be significantly degraded, i.e., the cliff effect occurs.

A considerably more complicated source coding method, such as HEVC-intra, would obtain a higher R-D performance compared with CCSDS-IDC or JPEG2000 at low PLR. However, the proposed method still outperforms HEVC-intra if the cliff effect occurs. As shown in Fig. 8, the reconstruction PSNR of HEVC-intra with Raptor code at a rate of $4/5$ degrades dramatically with PLR and is weaker than the proposed method at 0.05 PLR. The PSNR degradation of the proposed SBCS-PNQ-NLR is less sensitive to the PLR, which shows the robustness in unreliable channels. Although other CS-based coding and transmission schemes have no cliff effect, there is a PSNR gap from the proposed method. An example is 1.0 bpp at 0.5 PLR, where the proposed SBCS-PNQ-NLR still obtains 30.55 dB PSNR, much higher than the MS-BCS-SPL with 26.84 dB. Fig. 9 depicts the reconstructed Lena image with different PLRs. As the PLRs increase, the reconstructed image of SBCS-PNQ-NLR becomes smoother with the loss of some local texture details, such as the texture on the hat. However, other details, such as information on face and hair, appear to be effectively saved. This result shows that the proposed SBCS-PNQ-NLR is robust to packet loss.

This article has been accepted for publication in a future issue of this journal, but has not been fully edited. Content may change prior to final publication. Citation information: DOI 10.1109/TMM.2017.2774004, IEEE Transactions on Multimedia

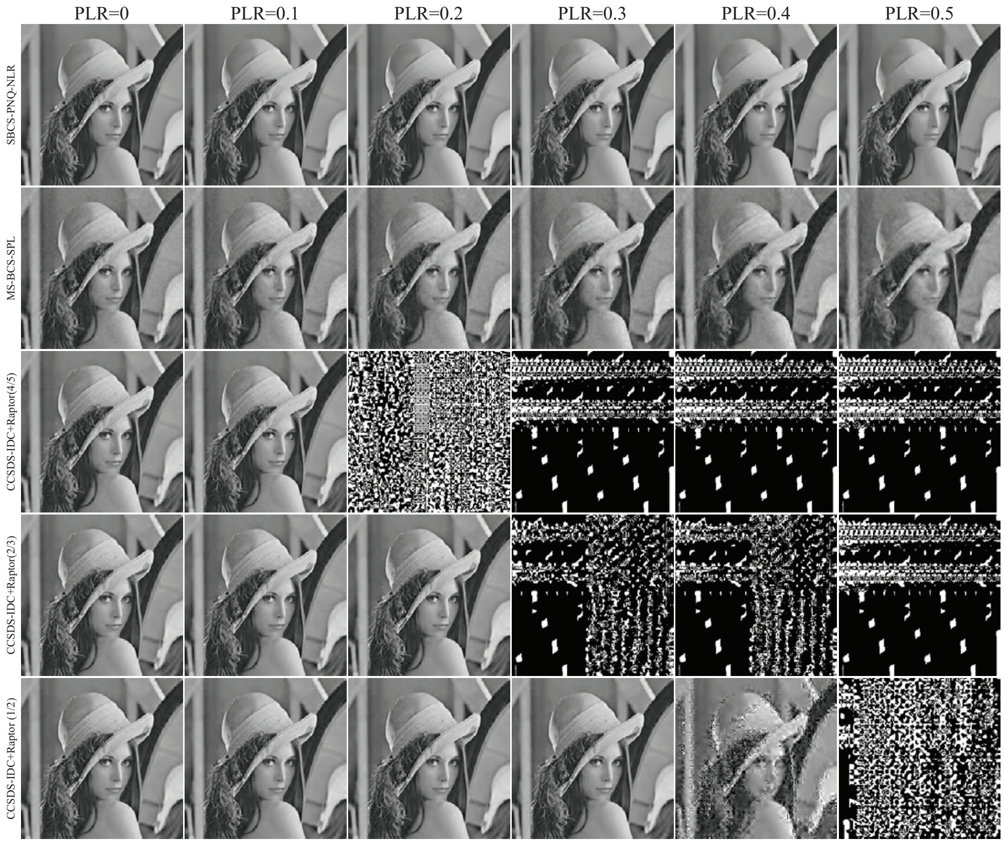

Fig. 9. Performance of SBCS-PNQ-NLR, MS-BCS-SPL and CCSDS-IDC+Raptor encoded at 1.0 bpp with different PLRs.

C. Encoder Complexity Comparison

We now compare the encoder running time of the proposed method with those of the traditional source coding method and other CS-based schemes. As the decoding process could be performed by powerful computers, the decoder complexity may not be a critical issue. The comparisons are performed using MATLAB 2010a on a typical PC equipped with a 3.3 GHz i5 processor with 8 GB of RAM. Traditional source coding encoders, including CCSDS-IDC, JPEG2000, and HEVC-intra, are written in C or C++. For the CS-based encoders, including SBCS-PNQ-NLR, BCS-SPL, MS-BCS-SPL, and TSW-CS, codes are written in MATLAB. There is no further optimization or parallel processing for the codes. The results are the average running times over forty-eight test images with different compression ratios. As demonstrated in TABLE III, the computational complexity of our SBCS-PNQ-NLR scheme is considerably lower than that of the state-of-the-art source image coding standards CCSDS-IDC, JPEG2000 and HEVC-intra. The SBCS-PNQ-NLR encoder only costs approximately one third of the CCSDS-IDC encoder time, which implies significantly lower computational complexity. Block-based CS frameworks, including SBCS-PNQ-NLR, BCS-SPL and MS-BCS-SPL, take much smaller encoder times than TSW-CS. among the block-based CS frameworks, MS-BCS-SPL has the largest complexity for its wavelet transform process. Although SBCS-PNQ-NLR costs slightly more than BCS-SPL, it has substantial R-D performance improvements.

TABLE III
ENCODER COMPLEXITY COMPARISON (S)

Method	bpp					
	0.5	1.0	1.5	2.0	2.5	3.0
SBCS-PNQ-NLR	0.0052	0.0073	0.0090	0.0110	0.0126	0.0143
BCS-SPL	0.0049	0.0060	0.0068	0.0079	0.0089	0.0101
MS-BCS-SPL	0.0108	0.0124	0.0137	0.0144	0.0160	0.0172
TSW-CS	0.1008	0.1858	0.2764	0.3480	0.4103	0.5045
CCSDS-IDC	0.0160	0.0210	0.0247	0.0280	0.0323	0.0353
JPEG2000	0.0392	0.0409	0.0419	0.0431	0.0439	0.0445
HEVC-intra	1.4930	1.5950	1.6750	1.7350	1.7840	1.8160

D. Discussion

1) Bit Allocation for Progressive Non-uniform Quantizer: The allocation of bits between the base and refinement layers in the progressive non-uniform quantizer plays a critical role in the R-D performance of the proposed CS compression transmission scheme. There are $\frac{\bar{m}B}{n}$ bpp allocated to the base layer, and the remaining $\frac{(m-\bar{m})b}{n}$ bpp are allocated to the refinement layer. Here, B and b are fixed at 5 and 3, respectively. Then, the compression ratio, denoted as R bpp, is given as follows:

$$R = \frac{\bar{m}B + (m-\bar{m})b}{n}. \tag{24}$$

For $\bar{m} \leq m \leq n$ and Eq. (24), the range of $\frac{\bar{m}B}{n}$ is given by

$$\max\{0, \frac{B}{B-b}(R-b)\} \leq \frac{\bar{m}B}{n} \leq R. \tag{25}$$

TABLE IV shows the average SBCS-PNQ-NLR reconstruction PSNR results of the tested images at different compression ratios with $\frac{\bar{m}B}{n}$ ranging from 0.45 to 0.85. The small change of $\frac{\bar{m}B}{n}$ would slightly affect the R-D performance. The underlined values are the corresponding reconstruction PSNRs with appropriate $\frac{\bar{m}B}{n}$. At low compression ratios, we prefer to allocate more bits to the base layer. For the 0.5 bpp compression ratio, $\frac{\bar{m}B}{n}$ is taken as 0.5, which means that all 0.5 bpp is allocated to the base layer. For the 1.0 bpp compression ratio, 0.6 bpp is allocated to the base layer. As the compression ratio increases, the base layer is allocated 0.75 bpp, and more bits are allocated to the refinement layer, which implies a smaller portion of bits allocated to the base layer. In conclusion, the $\frac{\bar{m}B}{n}$ can be taken as 0.5 and 0.6 for 0.5 bpp and 1.0 bpp, respectively, and the maximum between 0.75 and $\frac{B}{B-b}(R-b)$ for the compression ratio is greater than 1.0 bpp.

TABLE IV
THE AVERAGE PSNR (dB) RESULTS OF DIFFERENT BITS ALLOCATED TO THE BASE LAYER WITHIN PROGRESSIVE NON-UNIFORM QUANTIZER

Image	$\frac{\bar{m}B}{n}$	bpp					
		0.5	1.0	1.5	2.0	2.5	3.0
Average	0.45	31.07	35.08	36.74	37.73	38.28	38.49
	0.50	<u>30.94</u>	35.31	36.63	38.50	39.25	39.63
	0.55	-	35.42	37.51	38.85	39.66	40.09
	0.60	-	<u>35.43</u>	37.70	39.14	40.06	40.59
	0.65	-	35.36	37.77	39.30	40.30	40.91
	0.70	-	35.28	37.78	39.37	40.43	41.11
	0.75	-	35.17	<u>37.77</u>	<u>39.42</u>	<u>40.54</u>	<u>41.26</u>
	0.80	-	34.81	37.39	38.86	39.76	40.19
	0.85	-	34.73	37.40	38.95	39.90	40.38

2) Progressive Non-uniform Quantizer Performance: The contribution of the progressive non-uniform quantizer in the proposed SBCS-PNQ-NLR scheme is shown in TABLE V. Assume that SBCS and NLR are still employed for the sensing measurement and reconstruction, respectively. We test the performances of the progressive uniform quantizer, non-uniform quantizer and uniform quantizer for the progressive non-uniform quantizer. The average reconstruction PSNR results at 1.0 bpp are 35.43 dB, 34.93 dB, 34.37 dB and 33.45 dB for progressive non-uniform, progressive uniform, non-uniform and uniform quantizer, respectively. The progressive non-uniform quantizer, combining the advantages of the non-uniform quantizer and progressive uniform quantizer, leads to a higher PSNR performance.

TABLE V
AVERAGE PSNR (dB) RESULTS WITH DIFFERENT QUANTIZERS

Image	Quantization method	bpp					
		0.5	1.0	1.5	2.0	2.5	3.0
Average	**progressive non-uniform quantizer**	**30.94**	**35.43**	**37.77**	**39.42**	**40.54**	**41.26**
	progressive uniform quantizer	30.59	34.93	36.95	38.32	39.15	39.55
	non-uniform quantizer	30.94	34.37	36.00	37.09	37.85	38.30
	uniform quantizer	30.59	33.45	34.69	35.59	36.26	36.53

VI. CONCLUSION

This paper has proposed an efficient compressive sensing-based image coding and transmission scheme for visual sensor networks with limited resources over an unreliable and bandwidth-constrained channel. At the encoder side, scrambled image block compressive sensing with a separable sensing operator is proposed, which requires only a few add/sub operations while maintaining the democracy property. The progressive non-uniform quantization is developed to enhance the R-D performance. At the decoder side, we propose a progressive NLR reconstruction method, which exploits the non-local structured self-similarity and correlations among the measurements. The proposed scheme can achieve state-of-the-art coding efficiency with lower computational complexity at the encoder while showing robustness to packet loss.

ACKNOWLEDGEMENTS

This work was supported in part by the NSFC under Grant 61373113, u1531141, 61732008 and 61772407, the National Key R&D Program of China under Grant 2017YFF0107700, Guangdong Provincial Science and Technology Plan Project under Grant 2017A010101006 and 2016A010101005.

REFERENCES

[1] I. F. Akyildiz, T. Melodia, and K. R. Chowdury, “Wireless multimedia sensor networks: A survey,” *IEEE Wireless Communications*, vol. 14, no. 6, pp. 32–39, 2007.
[2] S. Soro and W. Heinzelman, “A survey of visual sensor networks,” *Advances in Multimedia*, vol. 2009, Art. no. 640386, Mar. 2009.
[3] X. Yuan, X. Wang, C. Wang, J. Weng, and K. Ren, “Enabling secure and fast indexing for privacy-assured healthcare monitoring via compressive sensing,” *IEEE Transactions on Multimedia*, vol. 18, no. 10, pp. 2002–2014, Oct. 2016.
[4] S. Pudlewski, A. Prasanna, and T. Melodia, “Compressed-sensing-enabled video streaming for wireless multimedia sensor networks,” *IEEE Transactions on Mobile Computing*, vol. 11, no. 6, pp. 1060–1072, 2012.
[5] Blue Book, No. 4, Consulative Committee for Space Data Systems (CCSDS) Recommendation for Space Data System Standard 122.0-B-1, 2005. [Online]. Available: http://public.ccsds.org/publications/BlueBooks.aspx
[6] S. Kokalj-Filipović and E. Soljanin, “Suppressing the cliff effect in video reproduction quality,” *Bell Labs Technical Journal*, vol. 16, no. 4, pp. 171–185, Apr. 2012.
[7] E. J. Candès, J. Romberg, and T. Tao, “Robust uncertainty principles: exact signal reconstruction from highly incomplete frequency information,” *IEEE Transactions on Information Theory*, vol. 52, no. 2, pp. 489–509, Feb. 2006.
[8] E. J. Candès and J. Romberg, “Robust signal recovery from incomplete observations,” in *2006 International Conference on Image Processing*, 2006, pp. 1281–1284.
[9] M. Davenport, J. Laska, and P. Boufounos, *A simple proof that random matrices are democratic.*, November 2009, [Online]. Available: http://dsp.rice.edu/cs.
[10] L. Y. Zhang, K.-W. Wong, Y. Zhang, and J. Zhou, “Bi-level protected compressive sampling,” *IEEE Transactions on Multimedia*, vol. 18, no. 9, pp. 1720–1732, Jun. 2016.
[11] V. K. Goyal, A. K. Fletcher, and S. Rangan, “Compressive sampling and lossy compression,” *IEEE Signal Processing Magazine*, vol. 25, no. 2, pp. 48–56, Feb. 2008.
[12] C. Deng, W. Lin, B. sung Lee, and C. T. Lau, “Robust image coding based upon compressive sensing,” *IEEE Transactions on Multimedia*, vol. 14, no. 2, pp. 278–290, Feb. 2012.
[13] Y. Wang, D. Wang, X. Zhang, J. Chen, and Y. Li, “Energy-efficient image compressive transmission for wireless camera networks,” *IEEE Sensors Journal*, vol. 16, no. 10, pp. 3875–3886, Oct. 2016.
[14] X. Song, X. Peng, J. Xu, G. Shi, and F. Wu, “Compressive sensing based image transmission with side information at the decoder,” in *2015 Visual Communications and Image Processing (VCIP)*, 2015, pp. 1–4.
[15] E. J. Candès and J. Romberg, “Sparsity and incoherence in compressive sampling,” *Inverse Problems*, vol. 23, no. 3, pp. 969–985, 2006.
[16] L. Gan, “Block compressed sensing of natural images,” in *2007 15th International Conference on Digital Signal Processing*, 2007, pp. 403–406.

This article has been accepted for publication in a future issue of this journal, but has not been fully edited. Content may change prior to final publication. Citation information: DOI 10.1109/TMM.2017.2774004, IEEE Transactions on Multimedia

[17] T. T. Do, T. D. Tran, and L. Gan, "Fast compressive sampling with structurally random matrices," in *2008 IEEE International Conference on Acoustics, Speech and Signal Processing*, 2008, pp. 3369–3372.

[18] T. T. Do, L. Gan, N. H. Nguyen, and T. D. Tran, "Fast and efficient compressive sensing using structurally random matrices," *IEEE Transactions on Signal Processing*, vol. 60, no. 1, pp. 139–154, Jan. 2012.

[19] Y. Rivenson and A. Stern, "Compressed imaging with a separable sensing operator," *IEEE Signal Processing Letters*, vol. 16, no. 6, pp. 449–452, Jun. 2009.

[20] H. Liu, B. Song, F. Tian, and H. Qin, "Joint sampling rate and bit-depth optimization in compressive video sampling," *IEEE Transactions on Multimedia*, vol. 16, no. 6, pp. 1549–1562, Jun. 2014.

[21] X. Li, X. Lan, M. Yang, J. Xue, and N. Zheng, "Universal and low-complexity quantizer design for compressive sensing image coding," in *2013 Visual Communications and Image Processing (VCIP)*, 2013, pp. 1–5.

[22] L. Wang, X. Wu, and G. Shi, "Binned progressive quantization for compressive sensing," *IEEE Transactions on Image Processing*, vol. 21, no. 6, pp. 2980–2990, Jun. 2012.

[23] S. Mun and J. E. Fowler, "Block compressed sensing of images using directional transforms," in *2009 16th IEEE International Conference on Image Processing (ICIP)*, 2009, pp. 3021–3024.

[24] J. E. Fowler, S. Mun, and E. W. Tramel, "Multiscale block compressed sensing with smoothed projected landweber reconstruction," in *Signal Processing Conference, 2011 19th European*, 2011, pp. 564–568.

[25] G. Coluccia, D. Valsesia, and E. Magli, "Smoothness-constrained image recovery from block-based random projections," in *2013 IEEE 15th International Workshop on Multimedia Signal Processing (MMSP)*, 2013, pp. 129–134.

[26] L. He and L. Carin, "Exploiting structure in wavelet-based bayesian compressive sensing," *IEEE Transactions on Signal Processing*, vol. 57, no. 9, pp. 3488–3497, Sept. 2009.

[27] W. Dong, G. Shi, X. Li, Y. Ma, and F. Huang, "Compressive sensing via nonlocal low-rank regularization," *IEEE Transactions on Image Processing*, vol. 23, no. 8, pp. 3618–3632, Aug. 2014.

[28] C. Duran-Faundez, V. Lecuire, and F. Lepage, "Tiny block-size coding for energy-efficient image compression and communication in wireless camera sensor networks," *Signal Processing: Image Communication*, vol. 26, no. 8–9, pp. 466–481, Aug. 2011.

[29] M. F. Duarte and R. G. Baraniuk, "Kronecker compressive sensing," *IEEE Transactions on Image Processing*, vol. 21, no. 2, pp. 494–504, Aug. 2012.

[30] S. S. Pradhan and K. Ramchandran, "Generalized coset codes for distributed binning," *IEEE Transactions on Information Theory*, vol. 51, no. 10, pp. 3457–3474, Oct. 2005.

[31] F. Zhai, S. Xiao, and L. Quan, "A new non-uniform quantization method based on distribution of compressive sensing measurements and coefficients discarding," in *Signal and Information Processing Association Annual Summit and Conference (APSIPA), 2013 Asia-Pacific*, 2013, pp. 1–4.

[32] A. Gersho and R. M. Gray, *Vector Quantization and Signal Compression*. Boston: Kluwer, 1992.

[33] S. Li and H. Qi, "A douglas-rachford splitting approach to compressed sensing image recovery using low-rank regularization," *IEEE Transactions on Image Processing*, vol. 24, no. 11, pp. 4240–4249, Nov. 2015.

[34] J. Cai, E. J. Candes, and Z. Shen, "A singular value thresholding algorithm for matrix completion," *SIAM Journal on Optimization*, vol. 20, no. 4, pp. 1956–1982, Jan. 2010.

[35] [Online]. Available: http://decsai.ugr.es/cvg/dbimagenes/

[36] [Online]. Available: http://www.image-net.org/

[37] (2016, Sep.) Dvb-h. [Online]. Available: http://www.dvb-h.org

[38] (2016, Sep.) 3gpp. [Online]. Available: http://www.3gpp.org

Zan Chen Zan Chen received his B.S. degree from Xi'an Jiaotong University in 2012. He is now pursuing his Ph.D. degree from Xi'an Jiaotong University, Xi'an, China. His research interest is image compressive sensing.

Xingsong Hou Xingsong Hou received his Ph.D. degree from Xi'an Jiaotong University, Xi'an, China, in 2005. From October 2010-2011, he was a Visiting Scholar at Columbia University, New York, USA. Now, he is a Professor with the School of Electronics and Information Engineering, Xi'an Jiaotong University. He is with the Key Laboratory for Intelligent Networks and Network Security, Ministry of Education. His research interests include video/image coding, wavelet analysis, sparse representation, sparse representation and compressive sensing, and radar signal processing.

Xueming Qian Xueming Qian received his B.S. and M.S. degrees from the Xi'an University of Technology, Xi'an, China, in 1999 and 2004, respectively, and his Ph.D. degree from Xi'an Jiaotong University, Xi'an, China, in 2008. He was awarded a Microsoft fellowship in 2006. From 1999 to 2001, he was an Assistant Engineer at Shannxi Daily. From 2008 until now, he has been a Faculty Member with the School of Electronics and Information Engineering, Xi'an Jiaotong University. He was a Visiting Scholar at Microsoft Research Asia from August 2010 to March 2011. He is with the Key Laboratory for Intelligent Networks and Network Security, Ministry of Education, and with the Smiles Laboratory, Xi'an Jiaotong University. His research interests include video/image analysis, indexing, and retrieval.

Chen Gong Chen Gong received his B.S. degree in electrical engineering and mathematics (minor) from Shanghai Jiaotong University, Shanghai, China, in 2005, and his M.S. degree in electrical engineering from Tsinghua University, Beijing, China, in 2008. He received his Ph.D. degree in Electrical Engineering from Columbia University in May 2012. Now, he is working at the University of Science and Technology of China. His research interests are in the area of channel coding and modulation techniques for wireless communications and signal processing.